Absorber Enrichment and Its Implication on the Performance of Lead-free $CsSnI_3$ Perovskite Solar Cells (PSCs) - A 1D-SCAPS Study

Tajudeen Ahmed , Ibrahim Taofiq , Enock Oladimeji * , Durojaiye Koffa

Posted Date: 1 August 2023

doi: 10.20944/preprints202308.0016.v1

Keywords: Lead-free perovskite solar cell; CsSnI3 perovskite; charge carrier recombination; absorber enrichment; optimization; power conversion efficiency

Article

Absorber Enrichment and Its Implication on the Performance of Lead-Free $CsSnI_3$ Perovskite Solar Cells (PSCs) - A 1D-SCAPS Study

Ahmed, T. O. [1,*], Ibrahim, T. T. [2], Oladimeji, O. E [2] and Koffa, J. D. [2]

[1] Solid State Physics Group, Department of Physics, Federal University Lokoja, Kogi State Nigeria.
[2] Theoretical Physics Group, Department of Physics, Federal University Lokoja, Kogi State Nigeria
* Correspondence: tajudeen.ahmed@fulokoja.edu.ng

Abstract: Extensive research efforts have been made over the last few years to proffer solution to the high recombination rate and stability issues associated with Sn-based perovskite solar cells. In line with this, we modeled caesium tin iodide ($CsSnI_3$)-based perovskite solar cell (PSC) with titanium (IV) oxide (TiO_2) and copper thiocyanate *(CuSCN)* as the electron and hole transport materials respectively by employing One-Dimensional Solar Cell Capacitance Simulator *(1D-SCAPS)*. For the $CsSnI_3$-based PSC, *n-i-p* planar configuration was employed and previously published relevant data were used for the simulation. The results obtained for the initially modeled PSC compared well with similar devices in the literature. Based on the established relationship between charge carrier lifetime and power conversion efficiency (*PCE*) of a solar cell, we varied defect density in the cesium tin iodide ($CsSnI_3$) from $10^{13}\ cm^{-3}$ to $10^{17}\ cm^{-3}$ and studied its influence on the performance parameters of the modeled $CsSnI_3$-based PSC. We find that the diffusion length and lifetime of charge carriers are significantly increased with decreasing defect density of the $CsSnI_3$ absorber. In this study, we report that it is possible to significantly reduce the dominated *Shockley-Read-Hall* (*SRH*) high recombination rate occurring in $CsSnI_3$ perovskite layer even at a low defect density of $10^{13}\ cm^{-3}$ by using a combination of $SnCl_2$ and Br^- as additive and dopant respectively for $CsSnI_3$ enrichment. This strategy ensured a reduced concentration of Sn^{4+} vacancy (V_{Sn}) in the $CsSnI_3$ absorber and an improved carrier lifetime beyond *0.05 ns* as obtained for the initially modeled $CsSnI_3$ *–based PSC* by a magnitude of the order of 10^3 while the diffusion length was improved from $1.1\mu m$ by a magnitude of the order of 10^2 for the enriched $CsSnI_3$ *–based PSC*. For the optimized $CsSnI_3$*–based PSC*, we recorded the following photovoltaic parameters: open-circuit voltage (V_{OC}) = *1.289 V*, short-circuit current density (J_{SC}) = $32.60\ mA.cm^{-2}$, fill factor (*FF*) = *83.56%* and *PCE* = *35.12%*.

Keywords: Lead-free perovskite solar cell; $CsSnI_3$ perovskite; charge carrier recombination; absorber enrichment; optimization; power conversion efficiency

1. Introduction

The conversion of sunlight into electricity through photovoltaic (*PV*) effect using solar cells stands out as a potential solution to the future global energy crisis and environmental pollution brought about by energy generation from fossil fuel and natural gas [1-3]. The capacity of globally installed *PV* devices has been increasing over the last two decades. In *2020*, the globally installed *PV* capacity amounted to *788 GW*, with *183 GW* and 191*GW* of new *PV* capacity installed in 2021 and 2022 respectively. This would amount to *1.5 TW* if over 350.6 *GW* were to be installed in *2023* [4,5]. This indicates that the first generation silicon solar cells and the second generation thin film technologies are not only widely accepted but have also dominated the global PV markets [5,6]. Although, these solar cells have power conversion efficiency (*PCE*) of more than *26%* and a lifespan of about *25 years*, they are however characterized by high cost and difficult preparation conditions [6,7]. Amongst the third generation solar cells, perovskite solar cells (*PSCs*) have attracted significant attention due to lower material costs and low-temperature solution processing. Thus, making their fabrication procedures easy and cost-effective [7]. A typical PSC consists of an absorber material sandwiched between an electron transport material (*ETM*) and a hole transport material *(HTM)*. The

 doi:10.20944/preprints202308.0016.v1

ETMs that are most commonly used in *PSCs* are n-type semiconductors such as TiO_2, *ZnO* and *PCBM* [8-11] while the *HTMs* that are most commonly used are organic *p-type* polymers such as *spiro-OMeTAD*, *PTAA*, *P3HT* and *PEDOT:PSS* [10, 12-14].

Reports have shown that *PSCs* offer *PCE* of *25.2%* which is comparable to those of Si and thin-film solar cells [7, 15, 16]. The unique optical and electronic properties of perovskites are responsible for the improvement in their performance [17]. However, despite the large efficiencies recorded, the organic hole transport materials (*HTMs*) used in conjunction with the perovskite (absorber) are responsible for their instability and increased processing costs [18].

In addition, organic *HTMs* are also susceptible to degradation over time under humidity due to external doping usually done to guarantee optimum *PCE* in *PSCs* [19]. No doubt these shortcomings of organic *HTMs* pose as obstacle to large-scale commercialization of PSCs, as such the search for efficient and cost effective *HTM* calls for the use of inorganic *HTMs* to enhance the life time of PSCs and reduce the fabrication cost simultaneously. Prior reports showed that inorganic *HTMs* such as *CuI* and Cu_2O have exhibited good mechanical and chemical stabilities with encouraging stable *PCEs* [20-22]. However, copper thiocyanate (*CuSCN*) proved to be a better alternative inorganic *HTM* compared with *CuI* and Cu_2O as a result of its improved stability and distinct chemical robustness arising from its polymeric structure [23-26]. *CuSCN* is an inorganic p-type semi-conductor which exists in two forms as *α-CuSCN* and *β-CuSCN* with *β-CuSCN* being readily available and more thermally stable. In addition to these, it possesses compatible and easy solution processing ability, chemical stability, and high-optical transparency [27]. Comparative cost and performance analyses showed *CuSCN* to be the right replacement for organic *HTMs* amongst various *HTMs* according to [18]. Over the years the *PCE* for *CuSCN*-based *PSCs* have increased from 12.4% [28] through 17.0% for pristine absorber and *CuSCN* films obtained via spray deposition [29] to 18% for low temperature solution processed *CuSCN* [30]. To date, research efforts are in progress to take the *PCE* for *PSCs* up to and beyond the maximum theoretical limit of efficiency formulated by Shockley–Queisser [31, 32]. Consequently, research efforts centered on theoretical modeling of *CuSCN*-based *PSCs* have been carried out to optimized their performance by varying the thickness, defect density, and effective valence band density of the absorber layer using *SCAPS* software [33-36]. Recently, the significance of shallow doping and diffusion length of absorber layer, valence band and conduction band offsets of the various active layers and interface defects was pointed out as being critical to the performance of *PSCs*. A thorough investigation vis-à-vis optimization of these critical factors was carried out with 1D-*SCAPS* leading to an optimized PCE of 25.20% for *PSC* using lead-based perovskite with *CuSCN* and TiO_2 as *HTM* and *ETM* respectively [18].

Due to environmental concerns and stringent conditions imposed on the use of lead material for electronic and *PV* devices, significant research efforts have been directed toward replacing lead with similar metals having comparable electronic and optical properties for the engineering of alternative metallic based halide perovskite [37, 38]. Accordingly, Ag^+, Bi^{3+}, Sb^{3+}, Ti^{4+}, Ge^{2+}, and Sn^{2+} have been proposed as replacement for lead because they are less toxic and possess comparable properties as lead [39-43]. Amongst the various alternatives, tin based organic halide perovskites such as $CH_3NH_3SnI_3$ (*MASnI₃*), $HC(NH_2)_2SnI_3$ (*FASnI₃*) have been considered more suitable for *PSCs* partly because tin belongs to the same group as lead and due to the record *PCE* reported for *PSCs* with tin based organic halide perovskites as absorber layers [28]. However, *PSCs* based on $MASnI_3$ and $FASnI_3$ have been found to be chemically unstable because the organic cations therein react with water molecules to form weak hydrogen bonds that degrade device upon longtime exposure to moisture, heat and light [44,45]. Recently, metallic based halide perovskites with Cs^+ cation have been investigated and found to be nontoxic with improved optoelectronic properties [46, 47]. Among the cesium based metallic halide perovskites, reports have shown $CsSnI_3$ to possess exceptional electrical and optical properties [48-58]. $CsSnI_3$ is a unique material that exhibits four polymorphs with two of them existing independently at room temperature. One of the room temperature phases is yellow (*Y*) with a one-dimensional double-chain structure and the other phase is black (*B-γ*) with a three-dimensional perovskite structure [59]. The black perovskite $CsSnI_3$ displays *p-type* metallic conductivity with unusually high conductivity when heat-treated and optical band gap of *1.3eV* [49,

Preprints (www.preprints.org) | NOT PEER-REVIEWED | Posted: 1 August 2023 doi:10.20944/preprints202308.0016.v1

59]. The ability of $CsSnI_3$ to emit strong near-infrared photoluminescence at room temperature has been attributed to the readily changing Sn vacancy centers in the structure [49]. This rare characteristic would present opportunity to discover visible and *IR* light-emitting materials at room temperature, suitable for achieving ground breaking applications in photovoltaics, radiation detectors, and light-emitting diodes because the perovskite structure can incorporate a broad range of elements [60].

In the light of the above and to eliminate the factors hindering the commercialization of *PSCs*, it is therefore of paramount importance to consider cesium tin iodide ($CsSnI_3$) as a replacement for lead-based perovskite in the engineering of *PSCs* with a strong focus on the optimization of critical physical factors that have direct influence on the *PCE*. The most urgent challenge of the $CsSnI_3$-based perovskite solar cell is their low V_{OC}, which is far behind the bandgap of $CsSnI_3$ perovskite (*1.3eV*). This is mainly due to the severe charge recombination and band alignment mismatch at the absorber layer and its interfaces with the transport layers. These limiting factors have been the main obstacle to the efficiency improvement of $CsSnI_3$-based perovskite solar cells. To further explore the photovoltaic potential of $CsSnI_3$-based perovskite solar cells, the most important task is to minimize charge carrier recombination by enriching the absorber layer. In this paper, a detailed and systematic investigation of a modeled *PSC* consisting of TiO_2 as *ETM* layer, $CsSnI_3$ as absorber layer and *CuSCN* as *HTM* layer has been carried out with emphasis on enrichment of absorber layer with a view to optimizing the device performance.

2. Theory

2.1. Theoretical Details

The transport of charge carriers through the perovskite absorber to the respective transport layers in a PSC is governed by the Poisson's equation and the continuity equations for electrons and holes as is the case of semiconductor [61]. Under solar light irradiation with a power intensity of P_{in}, the photogenerated charge carriers will flow inside the PSC in accordance with the continuity equations and their dynamics is governed by the following rate equation:

$$\frac{dn}{dt} = G - U \qquad (1)$$

where n is the concentration of charge carriers, *G* is the charge generation rate and *U* represents the overall recombination rate resulting from direct (band-to-band) and indirect (Shockley-Read-Hall) recombination.

At short-circuit condition, the total current density (J_{SC}) equals to the total charge collected with respect to the photon absorbed taking into account the losses due to various recombination mechanisms in the absorber and at the interfaces according to equation (2):

$$J_{SC} = J_0 \left[\exp\left(\frac{qV_{OC}}{k_B T} \right) - 1 \right] \qquad (2)$$

From equation (2), high absorption of incident photons is guaranteed if the energy of the photons is equivalent to the bandgap of the perovskite absorber and this ultimately leads to high V_{OC}. To sustain high V_{OC}, the perovskite absorber in the PSC should have low bulk and surface defects. The recombination current density (J_0) depends on the defect density, the charge carrier diffusion length and lifetime. As such, a minimum recombination rate is achievable with a reduced total defect density in the perovskite absorber layer, thus giving rise to longer lifetime ($\tau_{n,p}$) and diffusion length (*L*) of charge carriers necessary to improve the efficiency of the *PSC* as specified in the following relations:

$$\tau_{n,p} = \frac{1}{\sigma_{n,p} . \nu_{th} . N_t} \qquad (3)$$

and

Preprints (www.preprints.org) | NOT PEER-REVIEWED | Posted: 1 August 2023 doi:10.20944/preprints202308.0016.v1

$$L_{n,p} = \sqrt{D_{n,p} \cdot \tau_{n,p}} \quad (4)$$

where $\sigma_{n,p}$ is defect capture cross section for electrons and holes, v_{th} is thermal velocity of the charge carriers, N_t is the concentration of defects in the absorber layer and D is the diffusion coefficient indicating that diffusion length of charge carriers is proportional to their lifetimes. With a minimum recombination rate, the overall capability of a PSC specified by the fill factor (*FF*) in combination with enhanced V_{OC} will ultimately give rise to improved power conversion efficiency (η) usually quantified as follows:

$$\eta = \frac{FF.J_{SC}.V_{OC}}{P_{in}} \quad (5)$$

where the parameters (J_{SC}, V_{OC} and *FF*) determining the PCE (η) are extracted from the current density–voltage (*J–V*) curve of the PSC.

2.2. Cell Structure and Numerical Modeling

The n-i-p planar configuration was adopted for the PSC architecture and it comprises of five (5) layers which include FTO as the transparent conducting oxide layer (front contact), TiO_2 as the electron transport layer (ETM), $CsSnI_3$ as the absorber layer, CuSCN as the hole transport layer (HTM) and gold as the back metal contact. Figure 1(a) depicts the PSC architecture employed in this work while the corresponding band diagram for the components is shown in Figure 1(b).

The basic physical parameters for each layer are listed in Table 1, the optical reflectance at each interface was assumed to be zero and single distribution was adopted for the nature of the defect at the ETM/absorber and absorber/HTM interfaces respectively for the numerical simulation of the PSC. The absorption constant for the absorber is set as $10^4\,cm^{-1}$, Gaussian distribution was adopted for the nature of the defect in the absorber with characteristic energy as $0.1eV$ while the defect capture cross section for electrons and holes was set as $2\times10^{-14}\,cm^{-2}$. The simulation of the PSC was done under the standard conditions of irradiance of 1000 Wm^{-2} with $AM\ 1.5G$ and temperature of $300\,K$.

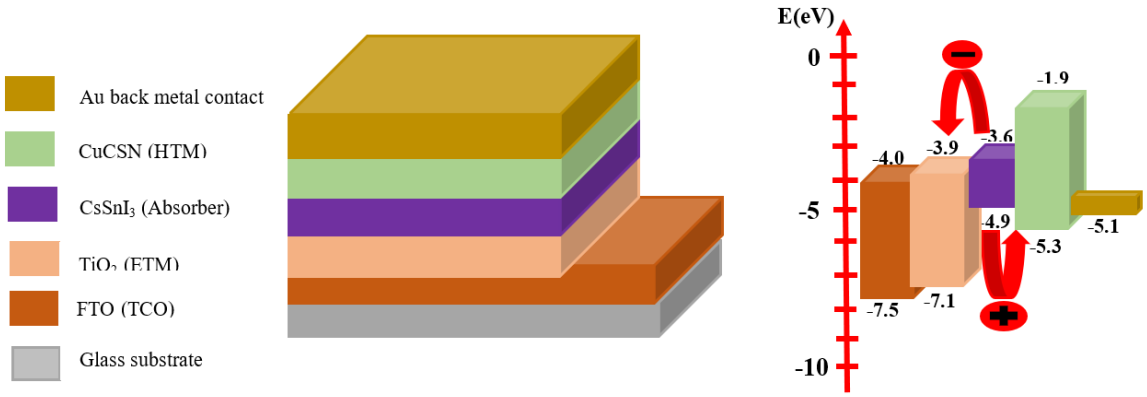

Figure 1. Schematic of the PSC structure (a) Device architecture and (b) Band diagram of the active layers.

Solar Cell Capacitance Simulator (SCAPS-1D) was employed to numerically simulate the proposed PSC architecture. The program takes into account only Shockley-Read-Hall (SRH) recombination statistics for the simulation and solves Poisson's equation together with the continuity equations for electrons and holes at each point in the proposed PSC subject to the imposed boundary conditions. To interpret the main limitations of the device current-voltage characteristics, the photovoltaic parameters of the cell were analyzed by varying the absorber layer thickness. Consequently, to deal with the recombination rate in the absorber layer, the defect density in the

Preprints (www.preprints.org) | NOT PEER-REVIEWED | Posted: 1 August 2023 doi:10.20944/preprints202308.0016.v1

perovskite absorber was varied from 10^{11} cm^{-3} to 10^{17} cm^{-3}. Finally, optimization of these parameters was done to improve the PCE of the modeled PSC.

Table 1. Parameters set for the simulation of Perovskite solar cell.

Parameters	FTO	TiO_2	$CsSnI_3$	CuSCN
Thickness (μm)	0.500	0.010	0.200	0.100
Band-gap energy E_g (eV)	3.5	3.2[63]	1.3[57]	3.40[64]
Electron affinity χ (eV)	4.0	3.9-4.8[65-67]	3.6[59]	1.9[68]
Relative Permittivity ε_r	9	38-108[69]	28[62]	9[70]
Effective conduction band density N_c (cm^{-3})	$2.2x10^{18}$	$2.2x10^{18}$ [71]	$1.57x10^{19}$[53]	$2.2x10^{18}$ [72]
Effective valence band density N_v (cm^{-3})	$1.8x10^{19}$	$1.8x10^{19}$ [71]	$1.47x10^{18}$[53]	$2.9x10^{19}$ [72]
Electron mobility μ_n (cm^2V^{-1} s^{-1})	20	20[73]	50[62]	$1x10^{-4}$ [74]
Hole mobility μ_p (cm^2V^{-1} s^{-1})	10	10[73]	585[57]	$1x10^{-2}$[74]
Donor concentration N_D (cm^{-3})	$2x10^{19}$	$1x10^{16}$	0	0
Acceptor concentration N_A (cm^{-3})	0	0	$1x10^{17}$[62]	$1x10^{18}$
Defect density N_t (cm^{-3})	$1x10^{15}$	$1x10^{17}$	$1x10^{17}$[53]	$1x10^{17}$

3. Results and Discussion

3.1. Initial PSC Simulation and Validation

The variation of the current density with applied voltage and the spectral response (quantum efficiency) of the simulated *$CsSnI_3$ –based* PSC are given as (*J–V*) and *QE* curves in Figures 2(a) and 2(b) respectively. With the applied voltage being scanned from *0* to *1.2 V*, charge carriers that are continuously generated with increasing intensity of the incident light during the simulation translated to nearly constant current density at lower voltages and at zero voltage it reaches a maximum value referred to as J_{SC} with a magnitude of *22.859 mA.cm*$^{-2}$ as shown in Figure 2(a). However, as the applied voltage increases, the recombination of charge carriers in the absorber and at the n/i interface of the simulated *$CsSnI_3$ –based PSC* became significant thus limiting the values of V_{OC} to *0.915 V*, as evident from Figure 2(a). The low V_{OC} is mainly due to charge recombination at the n/i interface and in the absorber of the simulated *$CsSnI_3$ –based PSC* as evident from high recombination rate in Figure 2(c). Also, the deviation of current-voltage characteristics of the simulated PSC from idealness brought about mainly by *SRH* recombination mechanism in the simulated device reduced the value of FF to *47.84%*. Thus, the overall PCE of the simulated PSC was obtained to be 10.*01%*. The simulated *QE* curve revealed that virtually all the photons from the incident light were absorbed from *385 nm* to *500 nm* of the wavelength range yielding *QE* of approximately *87%*. Beyond *500 nm*, the QE gradually reduced from 87% to *50%* at 821 *nm* and decreases sharply at about 950 nm, which corresponds to the band gap of $CsSnI_3$ thin film as a result of the competition between charge generation rate and charge recombination rate as evident from Figure 2(c). The strong optical absorption of the simulated *$CsSnI_3$ –based* PSC is attributed to the structural characteristics of *$CsSnI_3$* perovskite layer thus making it highly desirable for application in photovoltaics [59]. The obtained photovoltaic parameters for the simulated *$CsSnI_3$ –based* PSC agree fairly well with recently obtained results in the literature [75-79]. Though, the FF, V_{OC} and J_{SC} are lower compared to the same *$CsSnI_3$ –based* PSC with Spiro-OMETAD HTM [79], but the overall results for the simulated *$CsSnI_3$ –based* PSC with CuSCN HTM using the input parameters in Table 1 are better and higher than those previously obtained for *$CsSnI_3$ –based* PSC with polymer HTMs [80-86]. For the initial *$CsSnI_3$ –based* PSC, *0.2 μm* and *10^{17} cm^{-3}* have been employed for the thickness and defect density of the absorber respectively and the observed diffusion lengths (*0.08 μm* and *0.28 μm* for

Preprints (www.preprints.org) | NOT PEER-REVIEWED | Posted: 1 August 2023 doi:10.20944/preprints202308.0016.v1

electrons and holes respectively) are small due to high defect density in the absorber which ultimately limits charge carrier lifetime to *0.05ns* and eventually increases the recombination rate in the bulk of the initial *$CsSnI_3$ –based* PSC.

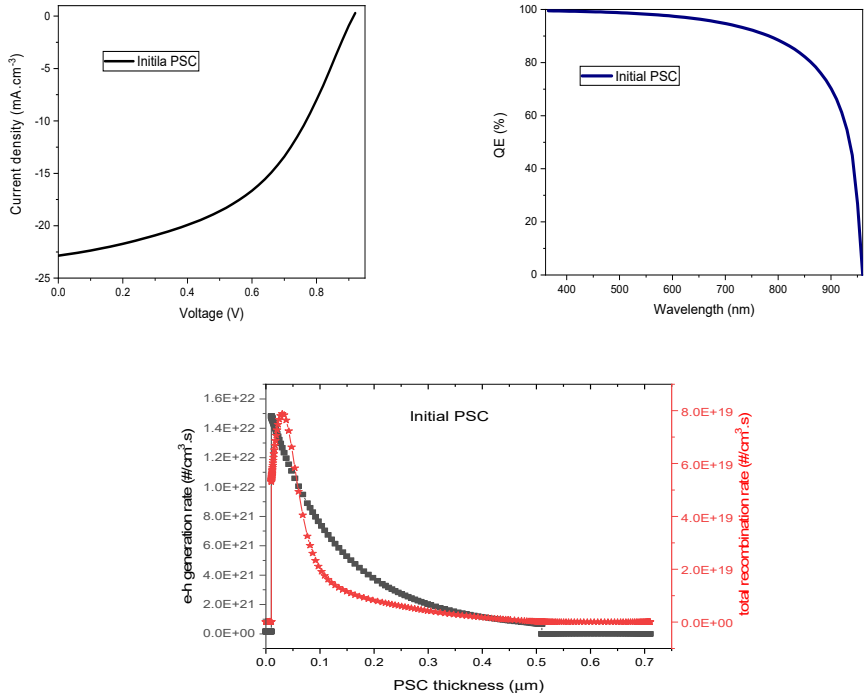

Figure 2. Performance characteristics of the simulated initial PSC (a) current density-voltage curve (b) quantum efficiency curve and (c) e-h generation and recombination rates.

To further explore the dynamics of charge carriers in the simulated *$CsSnI_3$ –based* PSC, the thickness of the absorber layer was varied from *0.1µm* to *1.0 µm* while maintaining the defect density at *10^{17} cm^{-3}* and the results obtained are presented in *Figure* 3. Accordingly, as more charge carriers are generated with increase in the absorber layer thickness, the rate of recombination charge carriers also increases due to reduced mobility brought about by high defect density as depicted in Figures *3(a)* and *3(b)*. This is evident from the reduction in the *V_{OC}* and *FF* as the absorber thickness increases. This trend is depicted in Figure *3(c)* and *3(d)* respectively with the *V_{OC}* reducing from a maximum value of *0.885V* for absorber thickness of *0.1µm* to a minimum value of *0.746V* for absorber thickness of *1.0µm* while the *FF* reduces from *75.29%* to *60.25%*. Nevertheless, enhancement in the values of the *J_{SC}* and *PCE* were observed which are in agreement with previous works on *$CsSnI_3$*-based PSC [78,79]. The results are presented in Figures *3(e)* and *3(f)* with *J_{SC}* increasing from *16.62 $mA.cm^{-2}$* to *34.48 $mA.cm^{-2}$* for absorber thickness of *0.1µm* and *1.0µm* respectively while the *PCE* increases from *11.074%* for absorber thickness of *0.1µm* up to 16.793% for absorber thickness of *0.5µm* followed by a gradual decrease to *15.506%* for absorber thickness of *1.0µm*.

Preprints (www.preprints.org) | NOT PEER-REVIEWED | Posted: 1 August 2023 doi:10.20944/preprints202308.0016.v1

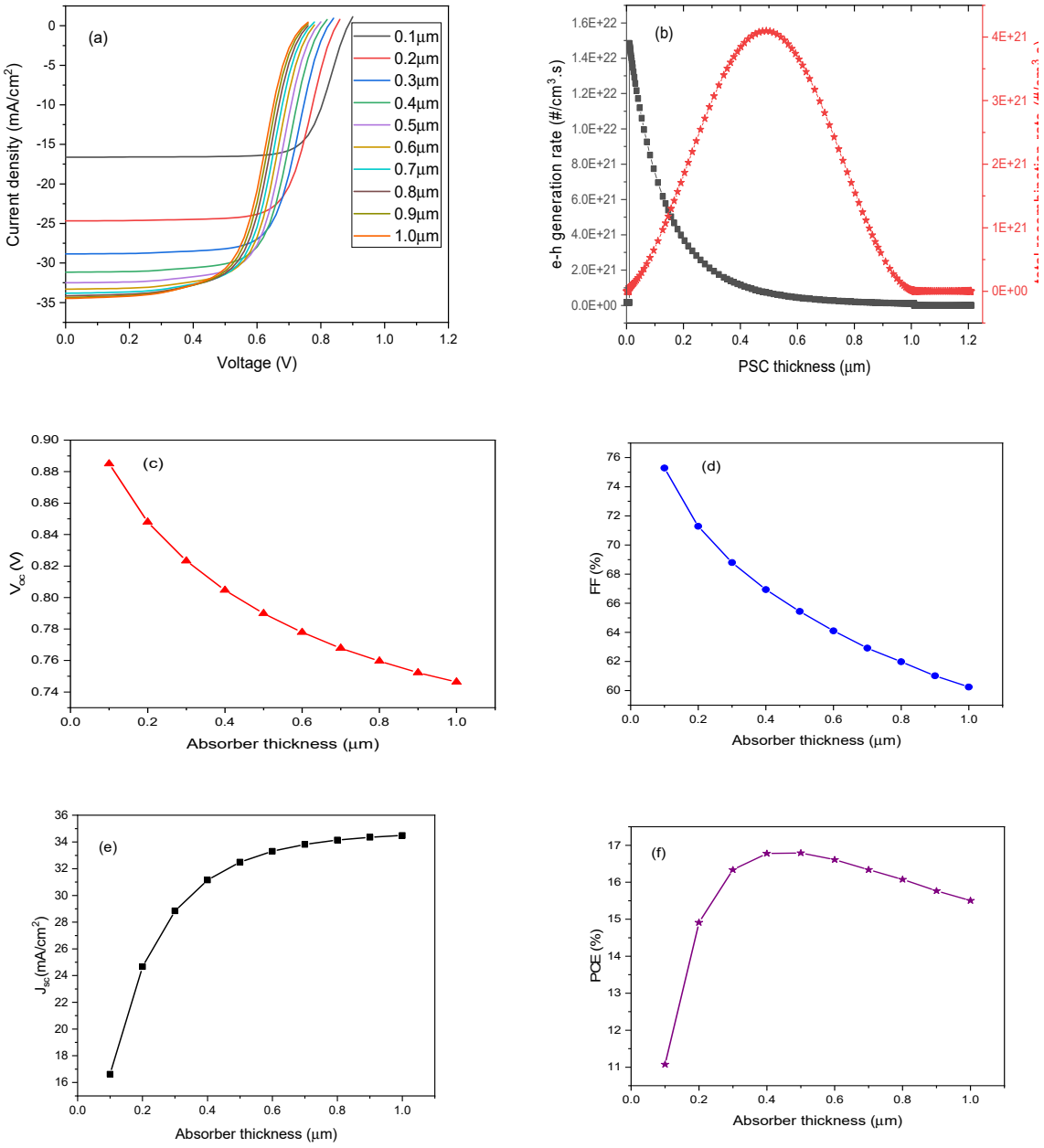

Figure 3. Variation of Performance parameters with absorber thickness (a) current density-voltage characteristics, (b) e-h generation and recombination rates and [(c)-(f)] photovoltaic parameters.

3.2. Absorber Enrichment and Device Optimization

To minimize charge carrier recombination rate and enhance V_{OC}, there is the need for compromise between the thickness of the absorber and its defect density, so that the diffusion length and the lifetime of charge carriers in the absorber are within the range required for uninterrupted transport and collection.

To achieve this, the defect density was tuned from $10^{11}\ cm^{-3}$ to $10^{17}\ cm^{-3}$ to gain an insight into the carrier transport dynamics with respect to the magnitude of enrichment of the absorber for real practical situations. With the results obtained from the variation of PCE with absorber thickness [*Figure 3(f)*], it was realized that it is pertinent to reduce the density of defects in the absorber of the simulated $CsSnI_3$-based PSC with thickness of $0.5\mu m$ and optimum *PCE*. The selected absorber thickness is in agreement with previous results obtained for simulated $CsSnI_3$–*based* PSCs using SCAPS software [78]. For selected thickness, the variation of the current density-voltage curves, the

Preprints (www.preprints.org) | NOT PEER-REVIEWED | Posted: 1 August 2023 doi:10.20944/preprints202308.0016.v1

charge carrier recombination rate of the $CsSnI_3$-based PSC and the photovoltaic parameters (J_{sc}, V_{oc}, FF and PCE) with the absorber defect density are presented in *Figure 4*. The current density remained constant with an average value of $32.60\ mA.cm^{-2}$ for the defect density range of interest as evident from *Figure 4(c)*. The carrier lifetime increases from *0.05 ns* to *50,000 ns* as the defect density drops from $10^{17}\ cm^{-3}$ *to* $10^{11}\ cm^{-3}$ and this increment translates to diffusion lengths that are long enough to improve photovoltaic parameters and the PSC performance. Correspondingly, improved values were observed for V_{OC}, *FF*, and *PCE* as the absorber defect density decreases from $10^{17}cm^{-3}$ to $10^{11}\ cm^{-3}$. *FF* has an optimum value of *80.13%* when the absorber defect density was reduced to $10^{13}\ cm^{-3}$ with an equivalent V_{OC} of *1.055 V* while the corresponding *PCE* value is *27.565%*. The need to reduce the noticeable high recombination rate at the n/i interface and in the absorber as depicted in *Figure 4(b)* is necessary in order to improve the V_{OC} and the *PCE* of the simulated $CsSnI_3$ *–based PSC* beyond the *Shockley-Queisser* limit. Although, the initiative demonstrated above is one of the important strategies needed for the lead-free *PSCs* to gain entry into the global PV markets but in real practical situations, it is difficult to synthesize $CsSnI_3$ absorber with a concentration of defect less than $10^{13}\ cm^{-3}$. This is because above room temperature, intrinsic defects are highly probable leading to the formation of significant concentration of Sn^{4+} vacancy (V_{Sn}) which in effect may promote recombination of holes with electrons in the stoichiometric $CsSnI_3$. Shallow doping of lead-free Sn-based perovskites using appropriate passivation additives (e.g., SnF_2, $SnCl_2$), reducing agents (hypophosphorous acid (*HPA*), hydrazine) and doping ions (Br^-, PEA^+, pn^+, and TN^+) have been reported in previous works to increase the formation energy of V_{Sn} and inhibit the oxidation of Sn^{2+} to Sn^{4+} [80-86]. In this work, it is therefore compelling to preserve the intrinsic properties and improve the stability of $CsSnI_3$ absorber layer through enrichment using a combination of $SnCl_2$ and Br^- with appropriate concentration as additive and dopant respectively. This strategy would ensure a reduced concentration of V_{Sn} and improve carrier lifetime beyond 0.05 ns as obtained for the initially simulated $CsSnI_3$*–based PSC*. For a fixed concentration of Sn^{+4} vacancy, if cesium iodide interstitials were filled with varying concentrations of Br^- and the bulk enriched with $SnCl_2$, then the formation energy of Sn^{+4} vacancy would increase and the oxidation of Sn^{+2} *to* Sn^{+4} would be inhibited. For this work, a novel strategy was employed by fixing $N_A=10^{14}\ cm^{-3}$, while N_V varies over a range of $10^{12}\ cm^{-3}$ to $10^{15}\ cm^{-3}$ and N_D also varies over a range of $10^{3}\ cm^{-3}$ to $10^{6}\ cm^{-3}$. Strategically, the equilibrium hole concentration in the enriched $CsSnI_3$ will decrease much more compared to that of the electron thereby making $CsSnI_3$ predominantly n-type. Thus, with N_C set to 10^{15} cm^{-3} and the optimum values for absorber thickness and total defect density (N_t) set to $0.5\mu m$ and $10^{13}\ cm^{-3}$ respectively, a reduced *SRH* recombination rate prevails leading to improved charge carrier collection efficiency and enhanced power conversion efficiency for the device. With these values, the *J-V* curves, *QE* curves and the photovoltaic parameters for the modified $CsSnI_3$-based *PSC* are given in Figure 5.

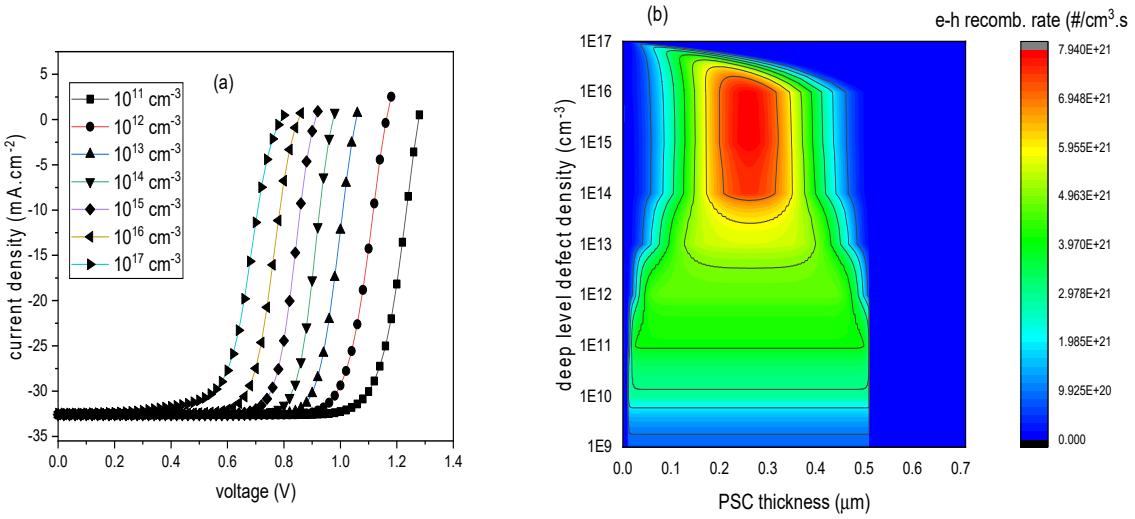

Preprints (www.preprints.org) | NOT PEER-REVIEWED | Posted: 1 August 2023 doi:10.20944/preprints202308.0016.v1

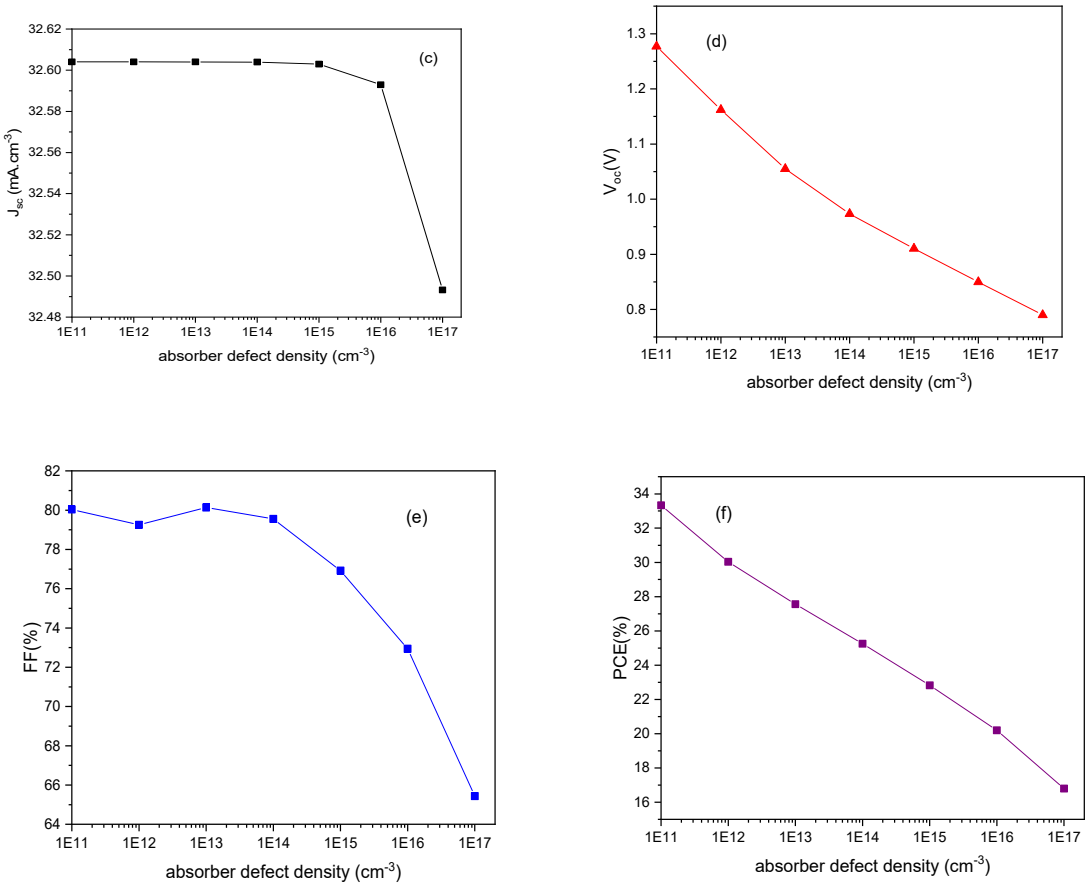

Figure 4. Variation of Performance parameters with absorber defect density (a) current density-voltage characteristics, (b) e-h recombination rates with PSC thickness and [(c)-(f)] photovoltaic parameters.

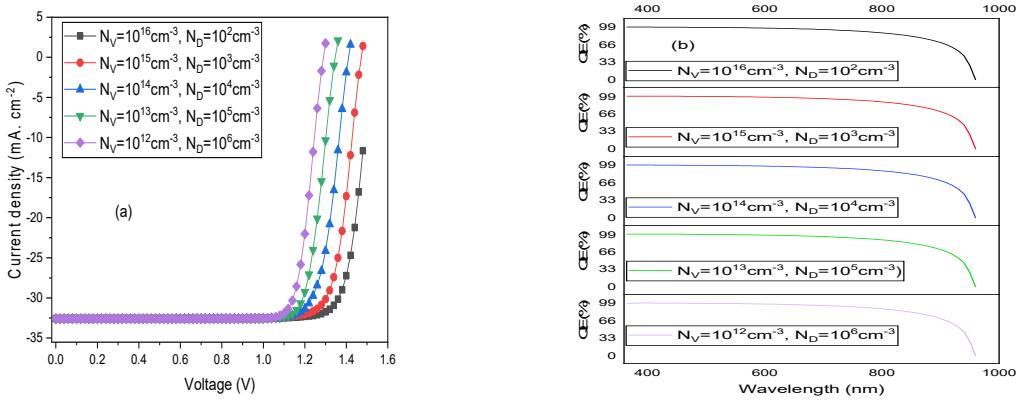

Preprints (www.preprints.org) | NOT PEER-REVIEWED | Posted: 1 August 2023 doi:10.20944/preprints202308.0016.v1

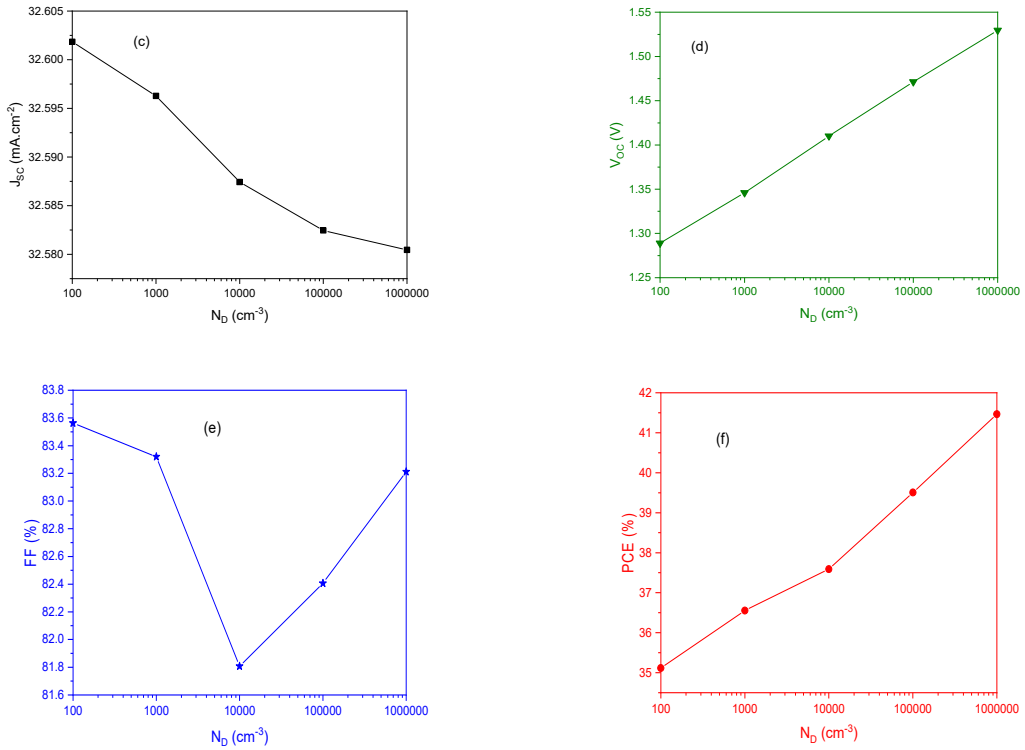

Figure 5. Variation of performance parameters for the modified *CsSnI*$_3$-based *PSC* with donor concentration (a) current density-voltage curves (b) Quantum efficiency curves (c) short-circuit current density (d) open-circuit voltage (e) Fill factor and (f) Power conversion efficiency.

Figure 6 compares the results obtained for the initial *CsSnI*$_3$-based *PSC* with that obtained for the optimized *CsSnI*$_3$-based *PSC*. The overall quality and idealness of the optimized *CsSnI*$_3$-based PSC are more pronounced compared to the initial *CsSnI*$_3$-based PSC as evident from the high fill factor (*FF*), enhanced open circuit voltage (V_{OC}) and short-circuit current density (J_{SC}) that ultimately gave rise to improved power conversion efficiency (PCE). From the J-V curves for the optimized *CsSnI*$_3$-based *PSC* and that for the initial *CsSnI*$_3$*–based* PSC given in Figure 6, we observed that the improvement in V_{OC} and J_{SC} for the optimized *CsSnI*$_3$-based *PSC* are approximately 29% and 30% respectively higher compared to those for the initial *CsSnI*$_3$-based *PSC* and this confirms efficient charge carriers transport and collection with minimal recombination rate. Thus, the resulting optimized *CsSnI*$_3$*–based PSC* performance parameters are V_{OC} = *1.289 V*, J_{SC} = *32.60 mA.cm*$^{-2}$, *FF = 83.56%* and *PCE = 35.12%*.

Preprints (www.preprints.org) | NOT PEER-REVIEWED | Posted: 1 August 2023 doi:10.20944/preprints202308.0016.v1

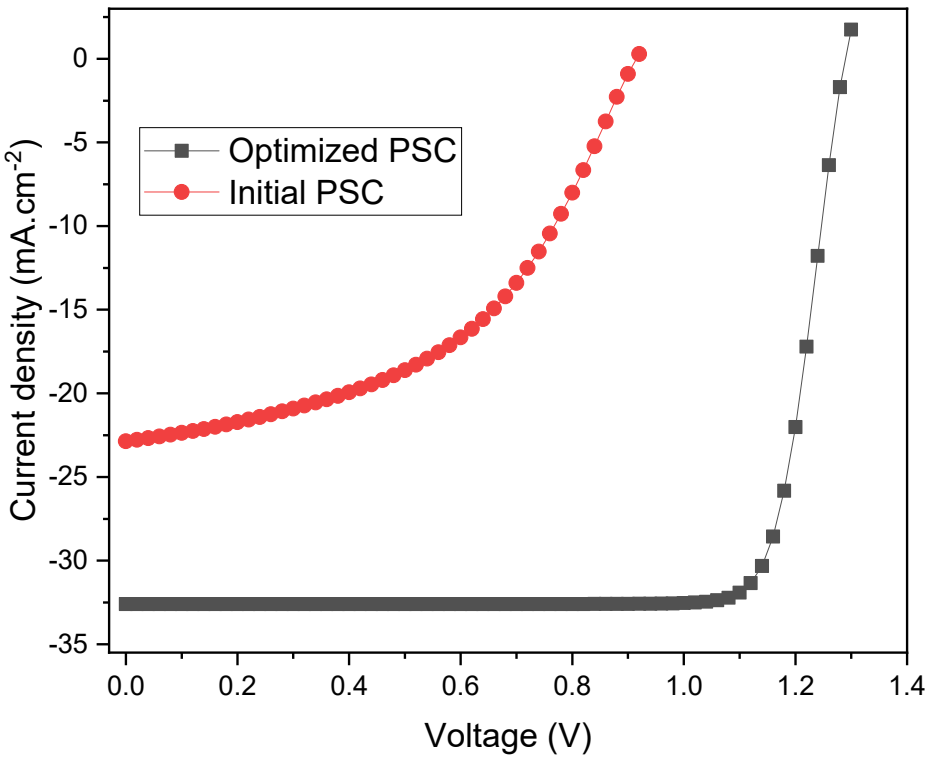

Figure 6. Current Density-Voltage Characteristics for the optimized and initial $CsSnI_3$-based *PSC*.

4. Conclusions

A systematic investigation of a modeled $CsSnI_3$-based *PSC* consisting of TiO_2 as *ETM* layer, $CsSnI_3$ as absorber layer and *CuSCN* as *HTM* layer was carried out with emphasis on enrichment of absorber layer with a view to optimizing the device performance using Solar Cell Capacitance Simulator (SCAPS-1D). For the initial $CsSnI_3$*–based* PSC, *0.2 µm* and 10^{17} cm^{-3} were employed for the thickness and defect density of the absorber respectively and the observed photovoltaic parameters were marred by high recombination rate of charge carriers thus limiting the values of J_{SC} to *22.859* $mA.cm^{-2}$, V_{OC} to *0.915 V*, *FF* to *47.84%* and *PCE* to 10.*01%*. To interpret the main limitations to the initial device current-voltage characteristics, the photovoltaic parameters of the cell were analyzed by varying the absorber layer thickness. Accordingly, a reduction in the values of V_{OC} and *FF* as the absorber thickness increases was evident while an enhancement in the values of the J_{SC} and *PCE* was observed. The *PCE* value increases from *11.074%* for absorber thickness of *0.1µm* up to an optimum value of 16.793% for absorber thickness of *0.5µm* and this was followed by a gradual decrease up to absorber thickness of *1.0µm*. Subsequently, the defect density in the perovskite absorber was varied from 10^{11} cm^{-3} to 10^{17} cm^{-3} to understand the recombination rate in the absorber layer. Correspondingly, improved values were observed for V_{OC}, *FF*, and *PCE* as the absorber defect density decreases from $10^{17}cm^{-3}$ to 10^{11} cm^{-3} while the current density remained constant with an average value of *32.60* $mA.cm^{-2}$ for the defect density range of interest. *FF* has optimum value of *80.13%* when the absorber defect density was reduced to 10^{13} cm^{-3} with an equivalent V_{OC} of *1.055 V* while the corresponding *PCE* value is *27.565%*. Finally, optimization of these parameters was done in conjunction with appropriate concentration of $SnCl_2$ and Br^- as additive and dopant respectively to improve the PCE of the modeled $CsSnI_3$-based PSC. This was achieved by fixing N_A=10^{14} cm^{-3}, while N_V varies over a range of 10^{12} cm^{-3} to 10^{15} cm^{-3} and N_D also varies over a range of 10^3 cm^{-3} to 10^6 cm^{-3}. Thus, with N_C set to 10^{15} cm^{-3} and the optimum values for absorber thickness and total defect density

(N_t) set to $0.5\mu m$ and $10^{13}\ cm^{-3}$ respectively, the resulting optimized *$CsSnI_3$–based PSC* performance parameters are $V_{OC} = 1.289\ V$, $J_{SC} = 32.60\ mA.cm^{-2}$, $FF = 83.56\%$ and $PCE = 35.12\%$ which represents an improvement over the initial results and compares reasonably well with results obtained from literature [78, 79, 84].

References

1. Wilson, G.M.; Al-Jassim, M.; Metzger, W.K.; Glunz, S.W.; Verlinden, P.; Xiong, G.; Mansfield, L.M.; Stanbery, B.J.; Zhu, K.; Yan, Y. The 2020 photovoltaic technologies roadmap. J. Phys. D Appl. Phys. 2020, 53, 493001. [CrossRef]
2. Singh, B.P.; Goyal, S.K.; Kumar, P. Solar PV cell materials and technologies: Analyzing the recent developments. Mater. Today Proc. 2021, 43, 2843–2849. [CrossRef]
3. METGroup. Renewable and Solar Energy Vs Fossil Fuels. Available online: https://group.met.com/en/mind-the-fyouture/mindthefyouture/solar-energy-vs-fossil-fuels (Accessed November 25, 2022).
4. PV Magazine. World has Installed 1 TW of Solar Capacity. Available online: https://www.pv-magazine.com/2022/03/15/humans-have-installed-1-terawatt-of-solar-capacity/ (Accessed 25 November, 2022); https://www.pv-magazine.com/2023/03/22/new-global-solar-capacity-additions-hit-191-gw-in-2022-says-irena/ (Accessed 17 May, 2023).
5. Statista. Global Cumulative Installed Solar PV Capacity 2000-2021. Available online: https://www.statista.com/statistics/280220/global-cumulative-installed-solar-pv-capacity/ (Accessed November 25, 2022).
6. Marques Lameirinhas, R.A.; Torres, J.P.N.; de Melo Cunha, J.P. A Photovoltaic Technology Review: History, Fundamentals and Applications. Energies **2022**, 15, 1823. [CrossRef]
7. Pastuszak, J.; Wegierek, P. Photovoltaic Cell Generations and Current Research Directions for Their Development. Materials **2022**, 15, 5542. [CrossRef]
8. Xiong, Y.; Liu, Y.; Lan, K.; Mei, A.; Sheng, Y.; Zhao, D.; Han, H. Fully printable hole-conductor-free mesoscopic perovskite solar cells based on mesoporous anatase single crystals New J. Chem. 2018, 42, 2669. [CrossRef]
9. Zhang, P.; Wu, J.; Zhang, T.; Wang, Y.; Liu, D.; Chen, H.; Ji, L.; Liu, C.; Ahmad, W.; Chen, Z. D.; Li, S. Perovskite Solar Cells with ZnO Electron-Transporting Materials. Adv. Mater. 2018, 30, 1703737. [CrossRef]
10. Jiang, T.; Fu, W. Improved performance and stability of perovskite solar cells with bilayer electron-transporting layers. RSC Adv. 2018, 8, 5897. [CrossRef]
11. Chen, S.; Yang, S.; Sun, H.; Zhang, L.; Peng, J.; Liang, Z.; Wang, Z. S. Enhanced interfacial electron transfer of inverted perovskite solar cells by introduction of CoSe into the electron-transporting-layer. J. Power Sources 2017, 353, 123. [CrossRef]
12. Jena, A. K.; Numata, Y.; Ikegami, M.; Miyasaka, T. Role of spiro-OMeTAD in performance deterioration of perovskite solar cells at high temperature and reuse of the perovskite films to avoid Pb-waste. J. Mater. Chem. A, 2018, 6, 2219-2230. [CrossRef]
13. Ng, C. H.; Ripolles, T. S.; Hamada, K.; Teo, S. H.; Lim, H. N.; Bisquert, J; Hayase, S. Tunable Open Circuit Voltage by Engineering Inorganic Cesium Lead Bromide/Iodide Perovskite Solar Cells. Sci. Rep. 2018, 8, 2482. [CrossRef]
14. Neophytou, M.; Griffiths, J.; Fraser, J.; Kirkus, M.; Chen, H.; Nielsen, C. B.; McCulloch, I. High mobility, hole transport materials for highly efficient PEDOT:PSS replacement in inverted perovskite solar cells. J. Mater. Chem. C, 2017, 5, 4940-4945. [CrossRef]
15. NREL. Best Research-Cell Efficiency Chart. Available online: https://www.nrel.gov/pv/cell-effienciency.html (accessed on 24 November 2022).
16. Sharma, P.; Goyal, P. Evolution of PV technology from conventional to nano-materials. Mater. Today Proc. **2020**, 28, 1593–1597. [CrossRef]
17. Baena, J.P.C.; Abate, A.; Saliba, M.; Tress,W.; Jacobsson, J.; Grätzel, M.; Hagfeldt, A. The rapid evolution of highly efficient perovskite solar cells. Energy Environ. Sci. **2017**, 10, 710–727. [CrossRef]

18. Haider, S. Z.; Anwar, H.; Wang, M. Theoretical Device Engineering for High-Performance Perovskite Solar Cells Using CuSCN as Hole Transport Material Boost the Efficiency Above 25%. Phys. Status Solidi A 2019, 216, 1900102. [CrossRef]
19. Kima, B. and Seok, S. I. Molecular aspects of organic cations affecting the humidity stability of perovskites. *Energy Environ. Sci.*, 2020, 13, pp. 805-820. [CrossRef]
20. Neophytou, M.; Griffiths, J.; Fraser, J; Kirkus, M.; Chen, H.; Nielsen, C. B.; McCulloch, I. High mobility, hole transport materials for highly efficient PEDOT:PSS replacement in inverted perovskite solar cells. J. Mater. Chem. C, 2017, 5, 4940-4945. [CrossRef]
21. Chen, W. Y.; Deng, L. L.; Dai, S. M.; Wang, X.; Tian, C. B.; Zhan, X. X.; Xie, S. Y.; Huang, R. B.; Zheng, L. S. Low-cost solution-processed copper iodide as an alternative to PEDOT:PSS hole transport layer for efficient and stable inverted planar heterojunction perovskite solar cells. J. Mater. Chem. A, 2015, 3, 19353-19359. [CrossRef]
22. Li, X.; Yang, J.; Jiang, Q.; Chu, W.; Zhang, D.; Zhou, Z.; Xin, J. Synergistic Effect to High-Performance Perovskite Solar Cells with Reduced Hysteresis and Improved Stability by the Introduction of Na-Treated TiO_2 and Spraying-Deposited CuI as Transport Layers
ACS Appl. Mater. Interfaces 2017, 9, 41354. [CrossRef]
23. Kumara, G.R.R.A.; Konno, A.; Senadeera, G.K.R.; Jayaweera, P.V.V.; De Silva, D.B.R.A.; Tennakone, K. Dye-Sensitized solar cell with the hole collector p-CuSCN deposited from a solution in n-Propyl sulphide. Sol. Energy Mater. Sol. Cells **2001**, 69, 195–199. [CrossRef]
24. Li, M.-H.; Yum, J.-H.; Moon, S.-J.; Chen, P. Inorganic p-Type Semiconductors: Their Applications and Progress in Dye-Sensitized Solar Cells and Perovskite Solar Cells. Energies **2016**, 9, 331. [CrossRef]
25. Hehl, R.; Thiele, G. Synthesis and Crystal Structure of $Me_3NHCu_2(SCN)_3$, $Me_2C{=}NMe_2Cu_2(SCN)_3$, and $Me_2C{=}NMe_2Ag_2(SCN)_3$. Three-dimensional Networks of Thiocyanatometallates(I). Zeitschrift für Anorganische und Allgemeine Chemie **2000**, 626, 2167–2172. [CrossRef]
26. Mahrov, B.; Hagfeldt, A.; Lenzmann, F.; Boschloo, G. Comparison of charge accumulation and transport in nanostructured dye-Sensitized solar cells with electrolyte or CuSCN as hole conductor. Sol. Energy Mater. Sol. Cells **2005**, 88, 351–362. [CrossRef]
27. Pattanasattayavong, P.; Ndjawa, G. O. N.; Zhao, K.; Chou, K. W.; Yaacobi-Gross, N.; O'Regan, B. C.; Amassian, A.; Anthopoulos. T. D. Electric field-induced hole transport in copper(i) thiocyanate (CuSCN) thin-films processed from solution at room temperature. Chem. Commun. 2013, 49, 4154-4156.
28. Yang, I. S.; Sohn, M. R.; Do Sung, S.; Kim, Y. J.; Yoo, Y. J.; Kim, J.; Lee, W. I.; Formation of pristine CuSCN layer by spray deposition method for efficient perovskite solar cell with extended stability. Nano Energy 2017, 32, 414.
29. Qin, P.; Tanaka, S.; Ito, S.; Tetreault, N.; Manabe, K.; Nishino, H.; Nazeeruddin, M. K.; Gratzel, M. Inorganic hole conductor-based lead halide perovskite solar cells with 12.4% conversion efficiency. Nat. Commun. 2014, 5, 1.
30. Jung, M.; Kim, Y. C.; Jeon, N. J.; Yang, W. S.; Seo, J.; Noh, J. H.; Seok, S. I. Thermal Stability of CuSCN Hole Conductor-Based Perovskite Solar Cells. ChemSusChem 2016, 9, 2592.
31. Anttu, N. Shockley–Queisser Detailed Balance Efficiency Limit for Nanowire Solar Cells
ACS Photonics 2015, 2, 446.
32. Sha, W. E. I.; Ren, X.; Chen, L.; Choy, W. C. H. The efficiency limit of $CH_3NH_3PbI_3$ perovskite solar cells. Appl. Phys. Lett. 2015, 106, 1.
33. Mostefaoui, M.; Mazari, H.; Khelifi, S.; Bouraiou, A.; Dabou, R. Simulation of High Efficiency CIGS Solar Cells with SCAPS-1D Software. Energy Procedia 2015, 74, 736.
34. Toshniwal, A.; Jariwala, A.; Kheraj, V.; Opanasyuk, A. S.; Panchal, C. J. Numerical Simulation of Tin Based Perovskite Solar Cell: Effects of Absorber Parameters and Hole Transport Materials jnep 2017, 9, 03038.
35. Haider, S. Z.; Anwar, H.; Wang, M. A comparative study of interface engineering with different hole transport materials for high-performance perovskite solar cells. Semicond. Sci. Technol. 2018, 33,35001.
36. Anwar, F.; Mahbub, R.; Satter, S. S.; Ullah, S. M. Effect of Different HTM Layers and Electrical Parameters on ZnO Nanorod-Based Lead-Free Perovskite Solar Cell for High-Efficiency Performance. Int. J. Photoenergy. 2017, 2017, 1-9.

37. Babayigit, A.; Duy Thanh, D.; Ethirajan, A.; Manca, J.; Muller, M.; Boyen, H.G.; Conings, B. Assessing the toxicity of Pb- and Sn-based perovskite solar cells in model organism Danio rerio. Sci. Rep., 2016, 6, 18721.
38. Li, J.; Cao, H. L.; Jiao, W. B.; Wang, Q.; Wei, M.; Cantone, I.; Lü, J.; Abate, A. Biological impact of lead from halide perovskites reveals the risk of introducing a safe threshold. Nat Commun. 2020, 11, 1, 310.
39. Islam, M. T.; Jani, M. R.; Al Amin, S. M.; Sami, M. S. U.; Shorowordi, K. M.; Hossain, M. I.; Devgun, M.; Chowdhury, A. S.; Bernajee, S.; Ahmed, S. Numerical simulation studies of a fully inorganic $Cs_2AgBiBr_6$ perovskite solar device. Optical Materials, 2020, 105, 109957.
40. Du, K., Meng, W., Wang, X., Yan, Y. & Mitzi, D. B. Bandgap Engineering of Lead-Free Double Perovskite $Cs_2AgBiBr_6$ through Trivalent Metal Alloying. *Angew. Chem. Int. Ed.* 56, 8158–8162 (2017).
41. Ju, M.-G.; Chen, M.; Zhou, Y.; Garces, H. F.; Dai, J.; Ma, L.; Padture, N. P.; Zeng, X. C. Earth-Abundant Nontoxic Titanium(IV)-based Vacancy-Ordered Double Perovskite Halides with Tunable 1.0 to 1.8 eV Bandgaps for Photovoltaic Applications. *ACS Energy Lett., 2018*, 3, 297–304.
42. Wang, N.; Zhou, Y.; Ju, M-G.; Garces, H. F.; Ding, T.; Pang, S.; Zeng, X. C.; Padture, N. P.; Sun, X. W. Heterojunction-Depleted Lead-Free Perovskite Solar Cells with Coarse-Grained B-γ-$CsSnI_3$ Thin Films. Adv. Energy Mater., 2016, 01, 130.
43. Canil, L.; Salunke, J.; Wang, Q.; Liu, M.; Köbler,H.; Flatken, M.; Gregori, L.; Meggiolaro, D.; Ricciarelli, D.; De Angelis, F.; Stolterfoht, M.; Neher, D.; Priimagi, A.; Vivo, P.; Abate, A. Halogen-Bonded Hole-Transport Material Suppresses Charge Recombination and Enhances Stability of Perovskite Solar Cells. Adv. Energy Mater., 2021, 01, 553.
44. Chen, M; Ju, M-G.; Garces, H. F.; Carl, A. D.; Ono, L. K.; Hawash, Z.; Zhang, Y.; Shen, T.; Qi, Y.; Grimm, R. L.; Pacifici, D.; Zeng, X. C.; Zhou, Y.; Padture, N. P. Highly stable and efficient all-inorganic lead-free perovskite solar cells with native-oxide passivation. Nature Commun., 2019, 10, 1, 6.
45. Shao, S.; Liu, J.; Portale, G.; Fang, H-H.; Blake, G. R.; Brink, G. H.; L. Jan Anton Koster, J. A.; Loi, M. A. Highly Reproducible Sn-Based Hybrid Perovskite Solar Cells with 9% Efficiency. Adv. Energy Mater., 2018, 8, 1702019.
46. Targhi, F. F.; Jalili, Y. S.; Kanjouri, F. MAPbI3 and FAPbI3 perovskites as solar cells: Case study on structural, electrical and optical properties. Results in Physics, 2018, 10, 616-627
47. Marshall, K. P.; Walker, M.; Walton, R. I.; Hatton, R. A. Enhanced stability and efficiency in hole-transport-layer-free $CsSnI_3$ perovskite photovoltaics. Nature Energy, 2016, 1, 16178.
48. Chung, I.; Lee, B.; He, J.; Chang, R.P.H.; Kanatzidis, M.G. All-Solid-State Dye-Sensitized solar cells with high efficiency. Nature **2012**, 485, 486–489. [CrossRef] [PubMed]
49. Wu, J.; Lan, Z.; Lin, J.; Huang, M.; Huang, Y.; Fan, L.; Luo, G. Electrolytes in Dye-Sensitized Solar Cells. Chem. Rev. **2015**, 115, 2136–2173. [CrossRef]
50. Bach, U.; Daeneke, T. A Solid Advancement for Dye-Sensitized Solar Cells. Angew. Chem. Int. Ed. **2012**, 51, 10451–10452. [CrossRef]
51. Mallouk, T.E. Applied chemistry: Molecules meet materials. Nature **2012**, 485, 450–451. [CrossRef] [PubMed]
52. Chen, Z.;Wang, J.J.; Ren, Y.; Yu, C.; Shum, K. Schottky solar cells based on $CsSnI_3$ thin-films. Appl. Phys. Lett. **2012**, 101, 093901. [CrossRef]
53. Shum, K.; Chen, Z.; Qureshi, J.; Yu, C.;Wang, J.J.; Pfenninger,W.; Vockic, N.; Midgley, J.; Kenney, J.T. Synthesis and characterization of $CsSnI_3$ thin films. Appl. Phys. Lett. **2010**, 96, 221903. [CrossRef]
54. Yu, C.; Chen, Z.J.;Wang, J.; Pfenninger,W.; Vockic, N.; Kenney, J.T.; Shum, K. Temperature dependence of the band gap of perovskite semiconductor compound CsSnI3. J. Appl. Phys. **2011**, 110, 063526. [CrossRef]
55. Chen, Z.; Yu, C.; Shum, K.; Wang, J.J.; Pfenninger, W.; Vockic, N.; Midgley, J.; Kenney, J.T. Photoluminescence study of polycrystalline $CsSnI_3$ thin films: Determination of exciton binding energy. J. Lumin. **2012**, 132, 345–349. [CrossRef]
56. Yamada, K.; Funabiki, S.; Horimoto, H.; Matsui, T.; Okuda, T.; Ichiba, S. Structural Phase Transitions of the Polymorphs of CsSnI3 by Means of Rietveld Analysis of the X-Ray Di_raction. Chem. Lett. **1991**, 20, 801–804. [CrossRef]
57. Chung, I.; Song, J.-H.; Im, J.; Androulakis, J.; Malliakas, C.D.; Li, H.; Freeman, A.J.; Kenney, J.T.; Kanatzidis, M.G. CsSnI3: Semiconductor or Metal? High Electrical Conductivity and Strong Near-Infrared

Photoluminescence from a Single Material. High Hole Mobility and Phase-Transitions. J. Am. Chem. Soc. **2012**, 134, 8579–8587. [CrossRef]

58. Zhou, Y.; Garces, H.F.; Senturk, B.S.; Ortiz, A.L.; Padture, N.P. Room temperature "one-Pot" solution synthesis of nanoscale CsSnI3 orthorhombic perovskite thin films and particles. Mater. Lett. **2013**, 110, 127–129. [CrossRef]
59. Chung, I.; Lee, B. H.; He, J.; Chang, R; Kanatzidis, M. G. All-solid-state dye-sensitized solar cells with high efficiency *Nature* 2012, 485, 7399, 486-9.
60. Sze, S.M.; Ng, K. Physics of Semiconductor Devices, John Wiley & Sons, 2006.
61. Kumar, M. H.; Dharani, S.; Leong, W. L. , Boix, P. P.; Prabhakar, R. R.; Baikie, T.; Shi, C.; Ding, H.; Ramesh, R.; Asta, M.; Graetzel M.; Mhaisalkar, S. G.; Mathews, N. Lead-free halide perovskite solar cells with high photocurrents realized through vacancy modulation. Adv. Mater. **2014,** 26, 7122-7127.
62. Wu, B.; Zhou, Y.; Xing, G; Xu, Q.; Garces, H. F.; Solanki, A.; Goh, T. W.; Padture, N. P.; Sum, T. C.. Long minority-carrier diffusion length and low surface-recombination velocity in inorganic lead-free $CsSnI_3$ perovskite crystal for solar cells. Adv. Funct. Mater. **2017**, 27, 1604818.
63. Pfeifer, V.; Erhart, P.; Li, S.; Rachut, K.; Morasch, J.; Brötz, J.; Reckers, P.; Mayer, T.; Rühle, S.; Zaban, A.; Mora Sero, I.; Bisquert, J.; Jaegermann, W.; Klein, A. Klein, Energy Band Alignment between Anatase and Rutile TiO_2 J. Phys. Chem. Lett. **2013**, 4, 4182– 4187
64. Wijeyasinghe, N.; Regoutz, A.; Eisner, F.; Du, T.; Tsetseris, L.; Lin, Y-H; Faber, H.; Pattanasattayavong, P.; Li, J.; Yan, F.; McLachlan, M.A.; Payne, D.J.; Heeney, M.; Anthopoulos, T.D. Copper(I) Thiocyanate (CuSCN) Hole-Transport Layers Processed from Aqueous Precursor Solutions and Their Application in Thin-Film Transistors and Highly Efficient Organic and Organometal Halide Perovskite Solar Cells. Adv. Funct. Mater. 2017, 27, 35.
65. Babaei, F. H.; Sheini, N. A.;. Lajvardi, M. M. Oxygen adsorption at noble metal/TiO_2 junctions. IOP Conference Series: Materials Science and Engineering, 2016, 108 (1), 012030.
66. Grover, S.; Moddel, G. Metal Single-Insulator and Multi-Insulator Diodes for Rectenna Solar Cells. 2013, Springer, 89-109.
67. Lajvardi, M. M.; Jahangiri, M.Ni/TiO2 ultraviolet detector IOP Conf. Ser. Mater. Sci. Eng. 2016, 108 (1), 012031.
68. Gavrilov, S. A.; Zheleznyakova, A. V.; Dronov, A. A.; Dittrich, T. Efficiency Enhancement of Eta-cells Fabricated by SILAR Deposition. Phy. Chem. Appl. Nanostructures, 2009, 577-580.
69. Boschloo, G.; Edvinsson, T.; Hagfeldt, A. Nanostructured Materials for Solar Energy Conversion. Elsevier, Amsterdam, 1st Edition, 2006.
70. Jaffe, J. E.; Kaspar, T. C.; Droubay, T. C.; Varga, T.; Bowden, M. E.; Exarhos, G. J. Electronic and Defect Structures of CuSCN. J. Phys. Chem. C 2010, 114, 9111-9117.
71. Zhao, T.; Shi, W.; Xi, J.; Wang, D.; Shuai, Z. Intrinsic and Extrinsic Charge Transport in $CH_3NH_3PbI_3$ Perovskites Predicted from First-Principles Sci. Rep. 2016, 7, 1.
72. Hossain, M. I.; Alharbi, F. H.; Tabet, N. Copper oxide as inorganic hole transport material for lead halide perovskite based solar cells. Sol. Energy 2015, 120, 370.
73. Zhang, Q.; Dandeneau, C. S.; Zhou, X.; Cao, G. ZnO nanostructures for dye-sensitized solar cells Adv. Mater. 2009, 21,4087.
74. Pattanasattayavong, P.; Promarak, V.; Anthopoulos, T. D. Electronic Properties of Copper(I) Thiocyanate (CuSCN). Adv. Electron. Mater. 2017, 3, 1600378.
75. Wang, Y.; Tu, J.; Li, T.; Tao, C.; Deng, X.; Li, Z. Convenient preparation of $CsSnI_3$ quantum dots, excellent stability, and the highest performance of lead-free inorganic perovskite solar cells so far. J. Mater. Chem. A 2019, 7, 7683–7690.
76. Ma, S.; Gu, X.; Kyaw, A. K.; Wang, D. H.; Priya, S.; Ye, T. Fully Inorganic $CsSnI_3$-based solar cells with>6% efficiency and enhanced stability enabled by mixed electron transport layer. ACS Appl. Mater. Interfaces 2021, 13, 1345–1352.
77. Li, B.; Di, H.; Chang, B.; Yin, R.; Fu, L.; Zhang, Y.; Yin, L. Efficient passivation strategy on Sn related defects for high performance all-inorganic $CsSnI_3$ perovskite solar cells. Adv. Funct. Mater. 2021, 31, No. 2007447.

78. Ye, T.; Wang, X.; Wang, K.; Ma, S.; Yang, D.; Hou, Y.; Yoon, J.; Wang, K.; Priya, S. Localized electron density engineering for stabilized B-γ $CsSnI_3$-based perovskite solar cells with efficiencies >10%. ACS Energy Lett. 2021, 6, 1480−1489.
79. Shuo L., Baoping Z., Tie-Yu L., Jin-Cheng Z., Huaqing P., Huanting C., Chuanjin L., Xirong L., Jinrong Z. Inorganic Lead-Free B-γ-$CsSnI_3$ Perovskite Solar Cells Using Diverse Electron-Transporting Materials: A Simulation Study. ACS Omega 2021, 6, 26689−26698
80. Song, T-B.; Yokoyama, T.; Stoumpos, C. C.; Logsdon, J.; Cao, D. H.; Wasielewski, M. R.; Aramaki, S.; Kanatzidis, M. G. Importance of reducing vapor atmosphere in the fabrication of Tin-based perovskite solar cells, J. Am. Chem. Soc., 2017, 139, 2, 836–842.
81. Song, T-B.; Yokoyama,T.; Aramaki, S.; Kanatzidis, M.G. Performance enhancement of lead-free tin-based perovskite solar cells with reducing atmosphere-assisted dispersible additive, ACS Energy Lett. 2017, 2, 4, 897–903.
82. Zhu, P.; Chen, C.; Gu, S.; Lin, R.; Zhu, J. $CsSnI_3$ Solar Cells via an Evaporation- Assisted Solution Method. Sol. RRL. 2018, 2, 4, 1–5.
83. Heo, J.H.; Kim, J.; Kim, H.; Moon, S.H.; Im, S.H.; Hong, K.H. Roles of SnX_2 (X=F, Cl, Br) additives in tin-based halide perovskites toward highly efficient and stable lead-free perovskite solar cells, J. Phys. Chem. Lett. 9 (20) (2018) 6024–6031.
84. Ban, H.; Zhang, T.; Gong, X.; Sun, Q.; Zhang, X-L.; Pootrakulchote, N.; Shen, Y.; Wang, M. Fully inorganic $CsSnI_3$ mesoporous perovskite solar cells with high efficiency and stability via coadditive engineering, Sol. RRL. 2021, 5, 7, 1–9.
85. Ye, T.; Wang, K.; Hou, Y.; Yang, D.; Smith, N.; Magill, B.; Yoon, J.; Mudiyanselage, R. H. H.; Khodaparast, G. A.; Wang, K.; Priya, S. Ambient-air-stable lead-free $CsSnI_3$ Solar cells with greater than 7.5% efficiency. J. Am. Chem. Soc. 2021, 143, 11, 4319–4328,
86. Ban, H.; Nakajima, T.; Liu, Z.;Yu, H.; Sun, Q.; Dai, L.; Shen, Y.; Zhang, X-L.; Zhu, J.; Chen, P.; Mingkui Wang, M. Over 8% efficient $CsSnI_3$-based mesoporous perovskite solar cells enabled by two-step thermal annealing and surface cationic coordination dual treatment, J. Mater. Chem. 2022, 10, 7, 3642–3649.